Adhesion of membranes and filaments on rippled surfaces

O. Pierre-Louis

CNRS/Rudolf Peierls Centre for Theoretical Physics, 1 Keble Road, Oxford OX1 3NP, United Kingdom

Adhesion of membranes and filaments on periodic rippled surfaces is studied by means of a one-dimensional model. The adhesion behavior is found to depend crucially on the shape of the ripples. Fakir-carpet and sinusoidal patterns are studied in detail. Infinite staircases of periodic ground states are found, with a periodicity diverging at a transition line. Moreover, the boundaries of the regions of existence of metastable states form a complex sequence on the fakir-carpet surface. This is inferred to lead to an unbinding transition by progressive stages when fluctuations are negligible. The occurrence of adhesion transitions for graphene, carbon nanotubes, and lipidic membranes is discussed quantitatively.

I. INTRODUCTION

When a liquid drop is in contact with a rough or patterned surface, two types of interface states are generically observed [1]. In the Wenzel state, the liquid is in contact everywhere with the substrate. In the Cassie-Baxter state, the interface is in contact with a fraction of the surface only, and another fluid (usually air) fills the asperities of the surface. The transition from one state to the other is observed experimentally [1]. It affects the static and dynamic properties of the drop.

In this paper, it is shown that soft objects, such as membranes or filaments, may also undergo similar transitions. Within the frame of a one-dimensional (1D) model, we focus on the case of a periodic rippled surface. We find that these transitions may occur either abruptly or by progressive stages. As an important difference from liquid surfaces, soft objects may exhibit a large number of metastable states, even for very simple periodic patterns.

Our first example of a "membrane" is graphene. Graphene has attracted much interest recently, mainly because of its special electronic properties. In experiments, graphene is usually observed in adhesion on a surface. The surface is often not perfectly flat, leading to an adhesion-induced graphene roughness. This roughness has important consequences, such as the suppression of weak-localization magnetoresistance [2]. Inspired by recent experiments of graphene on rough SiO_2 surfaces [3,4], we shall consider the case of graphene on rippled SiO_2. We will show that with a typical ripple wavelength of the order of 10 nm, graphene may exhibit free-standing bands between the ripples which are not in contact with the substrate. For larger-ripple wavelengths, graphene will follow the surface everywhere, and free-standing bands are not expected. The confinement of electrons into parallel bands on rippled surfaces is a crucial issue for the opening of an energy gap near the charge neutrality point for graphene [5]. Finally, using the results of Ref. [6], we suggest that adsorption of oxygen on graphene may lead to direct observation of adhesion transitions.

We also discuss the case of lipid membranes, without considering thermal fluctuations explicitly. The deformation of a lipid membrane in the vicinity of patterned [7] or rough [8] substrates was discussed in the literature in the limit where the deformation amplitude is smaller than the typical distance ℓ_{eq} to the substrate.

Here, the opposite limit is considered, where the membrane can wander far from the surface. The membrane-substrate interactions are then accounted for by means of a contact potential [9,10]. Such a limit is intrinsically nonlinear for two reasons. (1) Away from the substrate, the minimization of the curvature energy leads to a nonlinear differential equation. This problem is known as the Euler-Bernoulli elastica. (2) The adhesion geometry is free, and the positions of the contact points between the free parts and the adhering parts of the membrane are coupled in a nonlinear way. Previous work has indeed shown nonlinear behavior using a contact potential model adhesion of membranes onto objects of various geometries, such as atomic force microscope tips [11], pores [12], or colloids [13]. Here, we will use a small-slope approximation, which will linearize the equations for the parts of the membrane that are not in contact with the substrate, getting rid of the nonlinearity (1). But since the position of the contact points is still free, we keep the second origin of nonlinearity.[1] We shall see in the following how this leads to a complex behavior.

Filaments are also discussed within the same one-dimensional model. In doing so, we aim to describe a filament that is perpendicular to the ripples, neglecting lateral deformations and torsion.

We discuss the case of carbon nanotube adhesion quantitatively. The adhesion of carbon nanotubes on ripples is relevant for single-carbon-nanotube electronic devices, which are formed via deposition of nanotubes on linear electrodes which form ripples (or grids) [14]. We find that carbon nanotubes on rippled surfaces can undergo adhesion transitions within the range of experimentally relevant parameters [15], when the ripple wavelength is ∼50 nm.

Two different surface profiles are studied, fakir-carpet and sinusoidal surfaces. In each case, we determine all possible metastable states, and the ground state (i.e., the state with the lowest energy).

Fakir-carpet and sinusoidal surfaces both exhibit an infinite series of periodic ground states, with a period diverging

---

[1]The origin of the nonlinearity is the same as that encountered in the study of dendritic growth [31]: although the model is linear (the temperature field obeys the Laplace equation, and the boundary conditions are linear) the geometry is free, and this leads to complex nonlinear dynamics.

at a transition line. At this line, a transition to a floating ground state (i.e., not in contact with the substrate) is observed. Depending on the situation, the ground state may be the only stationary state, or may be accompanied by a plethora of metastable states. This should have some important consequences for the dynamics.

Furthermore, the knowledge of all metastable states allows us to draw some conclusion about quasistatic dynamics, which would result from the slow variation of model parameters when fluctuations and external perturbations are negligible. During quasistatic dynamics, the system has ample time to relax to a given metastable state, so that the dynamics is simply a list of metastable states which are successively explored. Hysteresis effects then come to the fore, and the system can be in a metastable state which is not the ground-state. As a first example, the observable unbinding transition on fakir-carpet surfaces occurs by progressive stages, involving progressive suppression of small-length-scale structures. In the following, this feature is called the "decimation sequence." No decimation sequence is found on sinusoidal surfaces. We also find hysteresis in the transition from partial adhesion to full adhesion on sinusoidal surfaces, a feature which is analogous to the metastability of the Cassie-Baxter state for liquid drops [1].

The model will be presented in Sec. II. In Sec. III, we explain the strategy for finding solutions in the small slope approximation. In Sec. IV, we discuss the results for the two different types of surfaces mentioned above. Section V is devoted to discussing whether the predicted transitions could occur in specific systems, such as graphene, carbon nanotubes, and lipidic membranes. Finally, we conclude in Sec. VI.

II. MODEL

A. Total energy

Using a simple 1D model, with curvature energy, tension, and contact adhesion, we shall focus on the case of a periodic rippled substrate. A rippled surface is defined as a surface for which $h_s(x,y) = h_s(x)$ is independent of y, where $h_s(x,y)$ is the surface height, and x, y are Cartesian coordinates parallel to the average orientation of the surface. Our model only accounts for the direction x, assuming translational invariance along y.

We start by defining the total energy as [9,10]

$$\mathcal{E} = \int ds \left(\frac{C}{2} \kappa(s)^2 + \sigma + V(\mathbf{r}(s)) \right), \tag{1}$$

where $\mathbf{r}(s)$ is the membrane position in the plane, s is the arclength, C is the bending rigidity, κ is the curvature [with the sign convention as shown in Fig. 1(a)], and $\sigma \geq 0$ is the tension. We do not consider the case $\sigma < 0$, which may lead to spontaneous buckling (such a situation could occur as a consequence of imposed excess area for the membrane, or as a consequence of a compressive stress).

The rigid solid and the membrane interact via the contact potential V: outside the solid $V=0$, at the surface $V=-\gamma$, and inside $V=+\infty$. Thus, γ is the adhesion energy, and the membrane cannot penetrate the solid. Self-crossing of the membrane is not considered explicitly in the model. We shall therefore simply exclude those configurations where the membrane crosses itself.
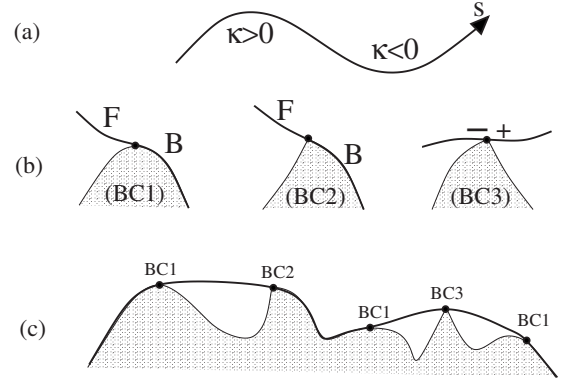

FIG. 1. (a) Sign convention for the curvature κ. (b) Three different types of boundary conditions (see text). (c) An example of a state composed of bridges linked by adhesion regions.

In the present work, we neglect the possibility for inhomogeneous stretching of the membrane or filament, and the related elastic energy. Our model can describe a liquid membrane (such as a lipidic one). It can also be valid for a solid membrane (such as a graphene sheet) if two conditions are satisfied. The first condition is that motion of the membrane along the surface is free. This means that we do not consider effects such as Coulomb friction, where a minimum force is needed in order to displace the membrane or filament along the surface. The second condition is of geometrical nature: the surface pattern must be a rippled pattern, so that the deformation is one dimensional, and inhomogeneous stretching can be avoided [16]. This would not be possible for an arbitrary two-dimensional pattern.

In the case of filaments, displacement along the interface should also be free for the stretching energy to be negligible. Moreover, we shall assume that the filament stays strictly perpendicular to the ripples. Hence, we will only consider "vertical" displacements of the filament (in the direction of the average surface normal). Finally, we neglect the effects of torsion.

We shall see in the next sections how a simple model based solely on the minimization of Eq. (1) already leads to a complex sequence of adhesion transitions.

B. Equilibrium equations

We look for local minima of the total energy, for which the variation $\delta\mathcal{E}$ vanishes. The equation $\delta\mathcal{E}=0$ leads to a differential equation for κ with boundary conditions (BCs). The derivation of these equations is reported in Appendixes A and B. In the free parts of the membrane, which are not in contact with the solid, κ obeys the Euler-Bernoulli elastica equation:

$$d^2 \left(\partial_{ss}\kappa + \frac{\kappa^3}{2} \right) - \kappa = 0, \tag{2}$$

where $d = (C/\sigma)^{1/2}$ is the length scale above which tension dominates over curvature effects.

There are three possible types of boundary conditions, as shown on Fig. 1(b). These boundary conditions are derived in Appendix A. In all cases, when $C \neq 0$, the membrane exhibits no angle at the contact point (i.e., its tangent is continuous across the contact point). Indeed, such an angle would lead to a divergence of the curvature energy (a discussion of this statement can be found in Ref. [17]).

In the first case (BC1), the substrate surface is locally smooth (no angle) and

$$\kappa_F = \kappa_B - \kappa_{eq}, \qquad (3)$$

where $\kappa_{eq} = (2\gamma/C)^{1/2}$, and κ_F and κ_B are the curvatures on the free and the bound sides, respectively. This boundary condition was already derived in the literature (see Refs. [9,10] and references therein).

The second case (BC2) corresponds to a membrane in contact with one of the sides of an angular point, and leads to

$$\kappa_B - \kappa_{eq} \leq \kappa_F \leq \kappa_B + \kappa_{eq}. \qquad (4)$$

Such a boundary condition is expected from the analogy to wetting, where the contact angle at an angular point obeys an inequality, which is known as the Gibbs inequality condition [18].

In the third case (BC3), the membrane is in contact with the substrate only at an angular point. In such a case the equilibrium of the torques imposes

$$\kappa_+ = \kappa_-, \qquad (5)$$

where $\pm$ indicates both sides of the contact point, as shown on Fig. 1(b). An additional condition is imposed by stability of the contact between the membrane and the surface:

$$\partial_s \kappa_+ \leq \partial_s \kappa_-. \qquad (6)$$

III. SMALL-SLOPE APPROXIMATION

A. Constructing small-slope solutions

Let us focus on the case of a periodic pattern, with a surface profile $h_s(x)$ of small amplitude $\sim \epsilon$ and period $\lambda \gg \epsilon$. The position of the membrane is $h(x) \geq h_s(x)$. In the small-slope approximation $\partial_x h \ll 1$, one may substitute s with x, and κ with $-\partial_{xx}h$ in Eqs. (2)–(6), and the κ^3 term in Eq. (2) is negligible.[2] Thus, Eq. (2) becomes linear:

$$d^2 \partial_{xxxx}h - \partial_{xx}h = 0. \qquad (7)$$

The general solution of this equation reads

$$h(x) = A_1 e^{x/d} + A_2 e^{-x/d} + A_3 x + A_4, \qquad (8)$$

where the A_i are constants.

A locally stable solution between two tangential contact points (i.e., with BC1 or BC2) is called a bridge. In order to determine the shape of the bridge, we have to find the four

constants of Eq. (8). These constants are obtained by matching the position and the slope of the bridges with the position and the slope of the substrate at the tangential contact points. Then, the boundary condition (3) provides us with two additional equations, which determine the position of the tangential contact points.

A bridge may have contact points with BC3 between the tangential contact points. The boundary conditions at this point are the following. First, the position of the membranes on both sides must be equal to the height of the contact point. Second, the slopes of the membrane on both sides of the contact point must be matched. Third, using Eq. (5), the curvatures must also be matched. With these conditions the shape of the whole bridge and the position of the contact points are again completely defined.

Bridges may then be linked with regions where the membrane is adhering to the surface (i.e. $h(x) = h_s(x)$), to form a "state" which exists everywhere along x. An example of such a state is shown in Fig. 1(c).

The state with the lowest energy is called the ground state, and the other states are called metastable states. In order to select the solutions which are physically relevant, we also have to eliminate the solutions which penetrate the solid, and those where the membrane exhibits self-crossing.

B. Validity of the small-slope approximation

The validity of the small-slope approximation can be analyzed in two limiting cases. The first case is the limit of vanishing tension $\sigma \to 0$. In such a case, BC1 imposes a curvature that must not induce large slopes for a height variation $\sim \epsilon$. This condition is written as

$$\epsilon \kappa_{eq} \ll 1. \qquad (9)$$

The second case is that of vanishing bending rigidity $C \to 0$, which corresponds to the usual wetting of liquids on solids. This limit is somewhat singular. Indeed, in the absence of bending rigidity, the interface can exhibit angles. As a consequence, the interface can be in contact everywhere with the substrate, even if the substrate exhibit angles (this is the so-called Wenzel state for liquids [1]). In such a state, $h(x) = h_s(x)$. Hence, the small-slope approximation $\partial_x h \ll 1$ requires small surface slopes: $\partial_x h_s \ll 1$. This latter condition is not satisfied for the fakir-carpet surface, where $\partial_x h_s$ diverges on the sides of the needles. Therefore, the limit $C \to 0$ cannot be taken for the fakir-carpet surface. Nevertheless, it can be taken for the sinusoidal surface, where small slopes can be achieved for a small enough amplitude of the patterns, as we shall see in Sec. IV B 2. Moreover, when $C \to 0$, BC1 must be replaced by the Young formula

$$\sigma[1 + \cos(\pi - \theta + \theta_s)] = \gamma, \qquad (10)$$

where $\tan \theta = \partial_x h$ and $\tan \theta_s = \partial_x h_s$. The angle $\pi - \theta - \theta_s$ is the usual contact angle. The small-slope condition then imposes $\theta - \theta_s \ll \pi$, so that the Young formula reduces to

$$\theta - \theta_s = \left(\frac{2\gamma}{\sigma} \right)^{1/2}. \qquad (11)$$

Therefore, we must also require $\gamma \ll \sigma$ for self-consistency.

---

[2]In order to prove this statement, we shall define a small parameter $\xi \ll 1$, so that $\partial_x h \sim \xi$. Moreover, we define the length scale ℓ_0 of the variations of h along x. Then $\kappa \sim \partial_x(\partial_x h) \sim \ell_0^{-1}\xi$. We therefore have $\kappa^3 \sim \ell_0^{-3}\xi^3 \ll \partial_{ss}\kappa \sim \ell_0^{-3}\xi$.
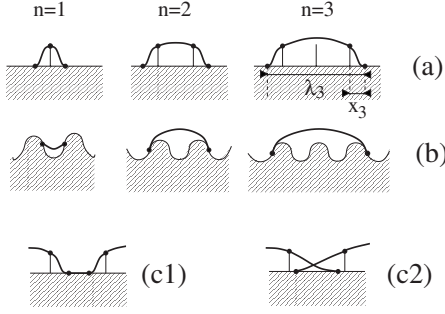
FIG. 2. A family of solutions called n-bridges ($n=1,2,3$, etc.) is found on the fakir-carpet (a) and the sinusoidal (b) surface. The lengths λ_3 and x_3 are shown in (a). These bridges are the only possible bridges. (c1) Non overlapping and (c2) overlapping adjacent bridges.

In the following, we shall assume that the small-slope approximation is valid. This assumption will be checked quantitatively on precise examples in Sec. V.

IV. RESULTS

A. Fakir-carpet surface

1. Bridge solutions

Let us first consider the fakir-carpet surface, with needles (or blades if the surface is 2D) of height ϵ separated by the distance $\lambda \gg \epsilon$. All the possible bridges are shown in Fig. 2(a). A detailed analysis of these solutions is presented on Appendix C. A bridge passing over n needles is called an n-bridge. Its total length is λ_n. The length $x_n=[\lambda_n-(n-1)\lambda]/2$ between the a tangential contact points with BC1, and the nearest needle with BC3 [see Fig. 2(a)] obeys:

$$0 = \zeta + \frac{\sinh[\beta x_n/\lambda + (n-1)\beta/2]}{\cosh[\beta x_n/\lambda + (n-1)\beta/2] - \cosh[(n-1)\beta/2]},$$

(12)

where

$$\beta = \frac{\lambda}{d} = \lambda \left(\frac{\sigma}{C}\right)^{1/2}$$

(13)

measures the relevance of tension at the scale of the wavelength λ of the pattern ($\beta \ll 1$ means negligible tension). Moreover, we have defined

$$\zeta = \frac{\beta^2/4\pi^2\alpha^2 + 1 - \cosh(\beta x_n/\lambda)}{\sinh(\beta x_n/\lambda) - \beta x_n/\lambda}.$$

(14)

The dimensionless number

$$\alpha = \left(\frac{\kappa_{\text{eq}}}{\kappa_g}\right)^{1/2} = \frac{\lambda}{2\pi\epsilon^{1/2}}\left(\frac{2\gamma}{C}\right)^{1/4}$$

(15)

compares the curvature κ_{eq} forced by BC1 or BC2, and the surface geometrical curvature $\kappa_g=4\pi^2\epsilon/\lambda^2$. When $\alpha \gg 1$, the membrane is expected to adhere everywhere along the surface. But when $\alpha \ll 1$, the membrane cannot adapt its shape to follow precisely that of the substrate. Partial or total unbinding is then expected.
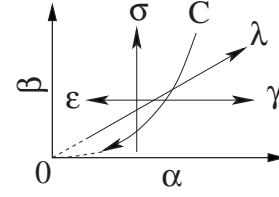

FIG. 3. The arrows show how one travels in the α, β plane when increasing one model parameter, with the other ones fixed.

As an example of solution of Eq. (12), one can evaluate the length $2x_1$ of a bridge on a surface with an isolated needle. From Eq. (12) one finds $x_1 \approx (6\epsilon/\kappa_{\text{eq}})^{1/2}$ for vanishing tensions ($\beta \ll \alpha$) and $x_1 \approx \epsilon\sigma^{1/2}/(2\gamma)^{1/2}$ for large tensions ($\beta \gg \alpha$). Let us now consider a surface with many needles separated by the distance λ. From the possible crossings or rearrangements of the bridges, we expect a nontrivial behavior when $x_1 \sim \lambda$. In the vanishing-tension limit, this condition reads $\alpha \sim 1$, as expected. In the large-tension limit, we obtain $\alpha \sim \beta^{1/2}$. With the help of Eq. (11), the latter condition may be rewritten as $\epsilon/\lambda \sim \theta - \theta_s$. This form leads to an intuitive interpretation: transitions will occur when the aspect ratio of the pattern is of the same order as the angle fixed by the Young boundary condition. These two scaling behaviors will be retrieved several times throughout the paper as the location of adhesion transitions.

In the following, results will systematically be plotted in the α, β plane. Figure 3 shows how we move in the α, β plane when varying one physical parameter, with the other parameters fixed.

The nonoverlapping condition for adjacent bridges with indices n and m, which forbids the situation shown on Fig. 2(c2), reads

$$x_n + x_m \lesssim \lambda.$$

(16)

This constraint may reduce the number of possible states. Here, it is not necessary to consider the condition of noncrossing of the membrane with the needles. Indeed, within our approximations, if two adjacent bridges do not overlap [as in Fig. 2(c1)], none of them crosses a needle.

2. Energy density

Periodic states composed of n-bridges only are denoted as nP. Their energy density G_n^f (i.e., energy per unit length) takes the form

$$G_n^f = \sigma + \gamma g_n^f(\alpha, \beta),$$

(17)

with

$$g_n^f(\alpha, \beta) = \frac{1}{n}\left(-1 + \frac{2x_n}{\lambda}\right) + \frac{2}{n\beta}(s_1 + \zeta c_1)^2 b$$
$$+ \frac{2}{n\beta}\left((1+\zeta^2)\frac{s_2}{2} + \zeta c_2 + \frac{\zeta x_n}{d} - 2\zeta c_1 - 2\zeta^2 s_1\right),$$

(18)

where $c_p=\cosh(p\beta x_n/\lambda)-1$, $s_p=\sinh(p\beta x_n/\lambda)$, $b=\coth[(n-1)\beta/2]$, and ζ is defined by Eq. (14).

For any state, we introduce the bridge distribution $\Phi = \{\phi_n ; n \geq 1\}$. Each ϕ_n is defined as the number of n-bridges divided by the total number of bridges, so that $\sum_{n=1}^{\infty} \phi_n = 1$. States having the same Φ have the same energy density, which is given by an equation similar to Eq. (17):

$$G^f(\Phi) = \sigma + \gamma g^f(\Phi, \alpha, \beta). \tag{19}$$

But now, the function g^f accounts for a linear superposition of energy densities of the periodic nP states

$$g^f(\Phi, \alpha, \beta) = \sum_{n=1}^{\infty} n \phi_n g_n^f(\alpha, \beta) \left(\sum_{n=1}^{\infty} n \phi_n \right)^{-1}. \tag{20}$$

Here, the expression (18) of g_n^f is used even when (16) forbids the nP state.

Since the energy density of the floating (F) state is $G_F = \sigma$, we obtain the adhesion energy of a given state, with a given bridge distribution Φ as

$$G^f(\Phi) - G_F = \gamma g^f(\Phi, \alpha, \beta). \tag{21}$$

Using Eq. (20), one may also show that the ground state is either the nP state with minimum g_n^f, or the F state.[3] Therefore, the ground-state is never composed of more than one type of bridge.

3. Ground states

The ground states of a membrane on the fakir-carpet surface are shown in Fig. 4(a), as a function of α and β. At weak tensions $\beta \ll 1$, an infinite staircase of nP states is found. At large α, the ground state is the $1P$ state. When decreasing α, the ground state successively becomes $2P$, $3P$, $4P$, etc. The index n of the nP ground state diverges for $\alpha = \alpha_\infty = 0.735\ldots$.

At large tensions $\beta \gg 1$, one finds

$$\alpha_\infty \approx \frac{\beta}{\pi(\beta - 3)^{1/2}}. \tag{22}$$

When increasing β, all the transition lines of the staircase converge exponentially fast to the line $\alpha = \alpha_\infty$, except for the transition from $n = 1$ to 2 which converges to

$$\alpha_1 \approx \frac{\beta}{\pi(\beta - 5)^{1/2}}, \tag{23}$$

so that the width $\alpha_\infty - \alpha_1 \approx \beta^{-1/2}/\pi$ decays like a power law with β. When $\alpha < \alpha_\infty$, the ground state is the F state.

These results indicate that the full staircase can be observed only for weak tensions. For larger tensions, only two lines, corresponding to α_∞ and α_1, will be observed.

---

[3]Assuming that G_n^f is minimum for $n = n^*$ and using Eq. (20), it is found that $G_\Phi^f \geq G_{n^*}^f$ for any Φ. Thus, n^*P is the ground state if it is allowed by the nonoverlapping condition (16). Overlapping of nP states occurs when $2x_n > \lambda$, which implies $g_n^f > 0$ from Eq. (18), so that $G_\Phi^f \geq G_{n^*}^f > \sigma = G_F$ for any Φ. Hence, F is the ground-state when n^*P is not allowed by (16).
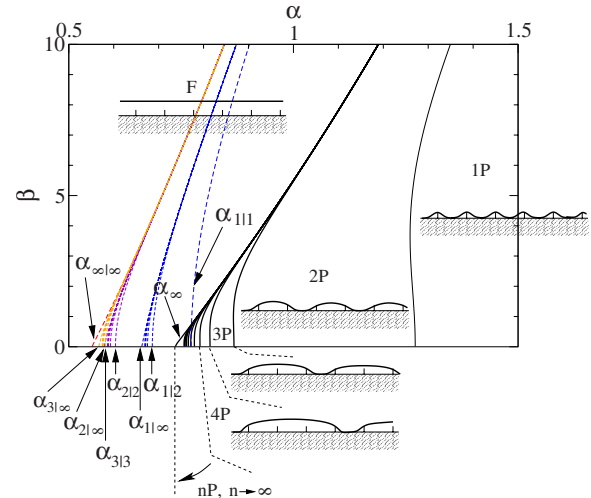

FIG. 4. (Color online) Phase diagram for the fakir-carpet surface. Solid lines separate different ground states. The nP ground states form an infinite staircase. Dashed line give the limit of existence of states. When $\alpha < \alpha_{\infty|\infty}$, the only state is F. When $\alpha > \alpha_{1|1}$, all states composed on n-bridges of Fig. 2(a) are possible.

4. Decimation sequence

Since states are locally stable by definition, the ground state transition lines in Fig. 4 are "first order," and a perturbation (which may be of thermal or external origin) is needed in order to go from one state to the other. When the model parameters are varied in the absence of perturbations, hysteresis effects can be observed. The observable transition is then rather the line where a state ceases to exist. On crossing this line, the system will switch to another state.

On the fakir-carpet surface, states cease to exist when two bridges overlap, as shown in Fig. 2(c). From (16), a couple of adjacent bridges n, m will overlap when $\alpha < \alpha_{n|m}(\beta)$, with $\alpha_{n|m}(\beta) = \alpha_{m|n}(\beta)$. A state will cease to exist (i.e., some adjacent bridges will overlap) when crossing the line $\alpha = \max[\alpha_{n|m}(\beta)]$, where the maximum is taken over all pairs n, m of adjacent bridges in the state.

From Eq. (12), one finds that x_n decreases monotonically when n increases. Using Eq. (16), it follows that

$$\alpha_{n+1|m}(\beta) < \alpha_{n|m}(\beta). \tag{24}$$

Thus, when α decreases, states containing bridges with low n will be decimated first. Moreover, decimation occurs in a region of finite width:

$$\alpha_{\infty|\infty}(\beta) < \alpha_{n|m}(\beta) \leq \alpha_{1|1}(\beta). \tag{25}$$

Note that the decimation order is tension dependent. As an example, $\alpha_{5|5}(0) < \alpha_{4|9}(0)$ and $\alpha_{5|5}(1) > \alpha_{4|9}(1)$. Hence, the first bridges to overlap in a given state may depend on the precise path in the α, β plane.

For large tensions $\beta \gg 1$, the lines $\alpha_{n|m}$ in the decimation region exponentially shrink to three lines at

$$\alpha_{1|1} \approx \frac{\beta}{\pi(2\beta - 8)^{1/2}}, \tag{26}$$

$$\alpha_{n|1} \approx \frac{\beta}{\pi(2\beta - 7)^{1/2}}, \quad n \geq 2, \tag{27}$$

$$\alpha_{n|m} \approx \frac{\beta}{\pi(2\beta - 6)^{1/2}}, \quad n,m \geq 2. \tag{28}$$

All decimation lines therefore converge to $\alpha_{1|1}(\beta) \approx \alpha_{\infty|\infty}(\beta) \rightarrow \beta^{1/2}/\pi\sqrt{2}$, and the total width of the region decreases as $[\alpha_{1|1}(\beta) - \alpha_{\infty|\infty}(\beta)] \rightarrow \beta^{-1/2}/2\pi\sqrt{2}$. As for the ground-state staircase, the decimation sequence can be observed fully for weak tensions only. For large tensions, three lines only can be observed.

We shall now focus on the region where $\alpha < \alpha_{\infty|\infty}$. In this region, the only possible state is F. Hence, there is no stationary configuration in contact with the substrate. Therefore, the membrane is expected to spontaneously unbind from the surface, without stopping in any intermediate state. We call such a system a "nonsticky" interface. In contrast, when $\alpha > \alpha_{\infty|\infty}$, the various ground states are accompanied by an infinite number of metastable states. Therefore, these ground states may be difficult to reach as the membrane may be trapped in other local minima.

Let us now assume that in an experiment we start with a random distribution of bridges at large α. The physical parameters are slowly varied such that the decimation staircase is crossed from the large- to the small-α region, up to the nonsticky F state. It is tempting to speculate that the system crossing the decimation region will undergo an unbinding transition by progressive stages, switching to states of larger and larger bridge lengths via the detachment of adhesion patches between the needles, and finally reaching the F state at $\alpha = \alpha_{\infty|\infty}$. A detailed analysis of this process would require a full dynamical model for membrane motion, and is beyond the scope of the present work.

B. Sinusoidal surfaces

1. Form and energy of the solutions

Let us now consider surfaces with a sinusoidal profile: $h_s(x) = \epsilon \sin(2\pi x/\lambda)$. Again, the derivation of the formulas presented in the main text is reported in Appendix D. As for the fakir-carpet surface, a single family of bridges—shown in Fig. 2(b)—is found, which obeys

$$\alpha^2 = |-\bar{c}_n + \beta\bar{s}_n/2\pi\bar{b}|, \tag{29}$$

where $\bar{c}_n = \cos(\pi\lambda_n/\lambda)$, $\bar{s}_n = \sin(\pi\lambda_n/\lambda)$, and $\bar{b} = \tanh(\lambda_n/2d)$. These solutions have the $x \rightarrow -x$ symmetry. They are centered either on a minimum or on a maximum of h_s (more precisely, a minimum for $n=1$, or $n \geq 2$ and even; and a maximum for $n \geq 3$ and odd).

The nP energy density ($n \geq 1$) still obeys Eq. (17), with

$$g_n^s(\alpha,\beta) = \left(1 - \frac{\lambda_n}{n\lambda}\right)\left(\frac{\alpha_c^4}{\alpha^4} - 1\right) + \frac{\bar{s}_n}{\pi n \alpha^4}$$
$$\times \left[\frac{\beta\bar{s}_n}{\pi\bar{b}} + \left(\frac{\beta^2}{4\pi^2} - 1\right)\bar{c}_n\right], \tag{30}$$
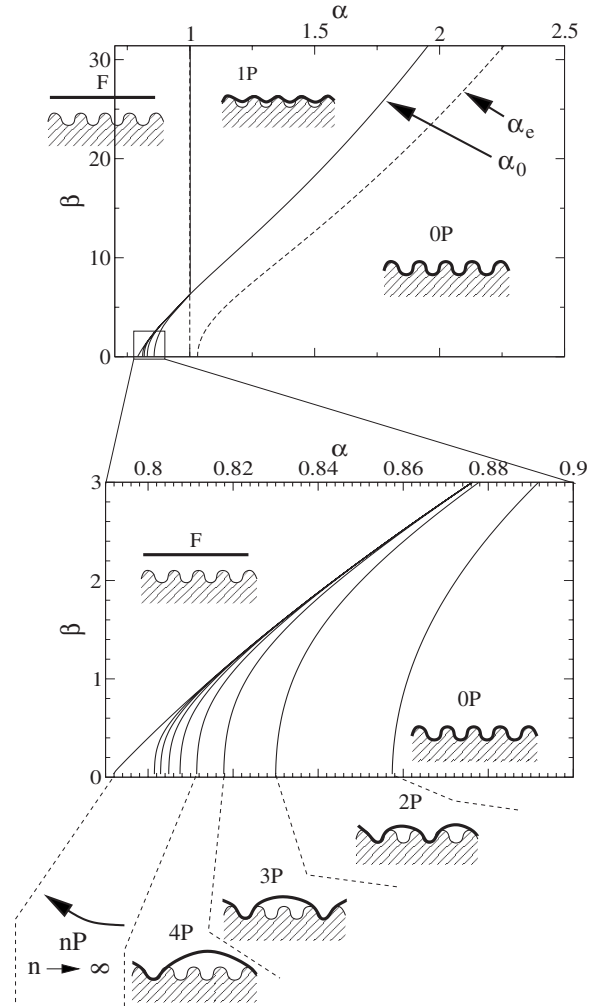
where

FIG. 5. Phase diagram for the sinusoidal surface. Solid lines separate different ground states. Dashed lines give the limits of existence of states. A small ground-state staircase is found. No decimation sequence of metastable states.

$$\alpha_c = (1 + \beta^2/4\pi^2)^{1/4}. \tag{31}$$

By convention, the state of full adhesion, where the membrane is everywhere in contact with the substrate is denoted as $0P$. Its energy density G_0^s takes the form (17), with

$$g_0^s(\alpha,\beta) = \frac{\alpha_c^4}{\alpha^4} - 1. \tag{32}$$

Finally, the superposition formula (20) still applies.

2. Ground states and metastable states

As in the case of the fakir-carpet surface, there is an infinite sequence of ground-state transitions. This feature occupies only a very small region on the full diagram, as shown in Fig. 5. In the rest of the diagram three ground states are found: F, $0P$, and $1P$. All ground-state transition lines cross at the point $(\alpha=1, \beta=2\pi)$.

The ground-state transition from the F state to the $1P$ state occurs at $\alpha=1$ and $\beta>2\pi$. The transition from the $1P$ to the $0P$ state occurs at $\alpha=\alpha_0$. For large tensions

$$\alpha_0 \approx (A\beta/2\pi)^{1/2}, \tag{33}$$

where $A \approx 0.78$ is a number that obeys:

$$2(\pi - \arcsin A)(A - 2/A) = (1 - A^2)^{1/2}. \tag{34}$$

All n-bridges with $n \geq 2$ exist for $\alpha \leq 1$. Therefore, as opposed to the case of the fakir-carpet surface, the F ground state coexists with many other states for small α. In contrast to the case of the fakir-carpet surface, we shall say that the interface is sticky for $\alpha \leq 1$: in the absence of fluctuations or external perturbations, the system may not find the F ground state, as it can be stuck in one of the numerous metastable states. Moreover, n-bridges with $n \geq 2$ do not exist for $\alpha > 1$ (see Appendix D for details). These bridges all cease to exist when crossing the line $\alpha = 1$.

The 1-bridge exists for $1 < \alpha < \alpha_e$. For large tensions ($\beta \gg 1$), we have

$$\alpha_e \approx (\beta/2\pi)^{1/2}. \tag{35}$$

From inspection of Fig. 5, it is seen that there is a region where the $1P$ state exists but is not the ground state. For large tensions, we may use Eqs. (33) and (35) and this region corresponds to $(A\beta/2\pi)^{1/2} < \alpha < (\beta/2\pi)^{1/2}$. Hence, when the line $\alpha = \alpha_e$ is crossed as α increases, the $1P \to 0P$ transition should be observed. But when the line $\alpha = \alpha_e$ is crossed by decreasing α, the $0P$ state should persist.

The above mentioned metastability region in fact corresponds to the well-known metastability of the Cassie-Baxter state for drops on superhydrophobic surfaces [1]. To see this, we shall first notice that the limit of drops, $C \ll 1$, corresponds to the region where $\beta \gg 1$. The transition line equations (33) and (35) may then be rewritten in a form that makes explicit their independence of the bending rigidity C in the limit $C \to 0$:

$$\left(\frac{\epsilon}{\lambda}\right)_0 = \frac{1}{2\pi A}\left(\frac{2\gamma}{\sigma}\right)^{1/2}, \tag{36}$$

$$\left(\frac{\epsilon}{\lambda}\right)_e = \frac{1}{2\pi}\left(\frac{2\gamma}{\sigma}\right)^{1/2}. \tag{37}$$

It must be noticed that the right-hand side (RHS) of these equations is related to the Young contact angle via Eq. (11).

In summary, we obtain that (i) for large aspect ratios $(\epsilon/\lambda) > (\epsilon/\lambda)_0$, the Cassie-Baxter ($1P$) state is the ground state; (ii) for intermediate aspect ratios $(\epsilon/\lambda)_0 < (\epsilon/\lambda) < (\epsilon/\lambda)_e$, the Wenzel ($0P$) state is the ground state, but the Cassie-Baxter ($1P$) state is metastable; and (iii) for smaller aspect ratios $(\epsilon/\lambda) < (\epsilon/\lambda)_e$, the Wenzel ($0P$) state is the ground state, and the Cassie-Baxter ($1P$) state is unstable.

V. DISCUSSION

A. Graphene

Graphene layers have been the subject of numerous studies in recent years. One of the important technological issues for graphene is the opening of an energy gap for electrons. Recent experiments on graphene ribbons show the appearance of a gap due to lateral confinement [5]. Another possibility is to deposit graphene on a rippled surface, thereby inducing free-standing bands of graphene above the bottom of the ripples, separated by adhesion regions on the top of the ripples [19], as, e.g., obtained for the $1P$ state of Fig. 4(b).

We shall discuss the case of graphene on a rippled SiO_2 surface, where $C = 0.9$ eV [6]. Recent experiments [3,4] suggest that $\gamma \sim 6$ meV $\mathring{A}^{-2}$. Moreover, we shall assume that graphene can freely slide along the surface, so that $\sigma \approx 0$.

Choosing a pattern with $\epsilon = 1$ nm, and $\lambda = 10$ nm, one finds $\alpha \sim 2$, right in the transition region. For ripples of the order of 10 nm or smaller, free-standing bands can be obtained. This is a rigorous statement on the fakir-carpet surface, where the F state is the only state at small wavelengths (i.e., small α). On the sinusoidal surface, this is only a tendency. Indeed, the $0P$ ground state can still be present, but it is unfavorable energetically.

For large ripple spacings (larger than 100 nm), we expect that graphene will follow the surface. This is rigorously true for sinusoidal surfaces, where no other state than the $0P$ state exists. But this is only a tendency for the fakir-carpet surface, where many other possible states coexist with the $1P$ ground state.

For the small-slope approximation to be valid, we need $\epsilon \kappa_{eq} < 1$. In the case of graphene, this condition reads $\epsilon < 0.9$ nm. Therefore, the small-slope approximation is valid for patterns of very small amplitude only. Indeed, for $\epsilon = 1$ nm as assumed previously, we have $\epsilon \kappa_{eq} \approx 1$. Moreover, the adhesion energy is not known precisely [3,4]. Therefore, our analysis provides orders of magnitude rather than precise numbers.

Adhesion of oxygen on graphene allows one to tune the bending rigidity continuously [6]. Using graphene rigidified with 12.5% oxygen, one would have $C = 40$ eV [6]. By increasing continuously the oxygen coverage on a surface with $\epsilon = 1$ nm, and $\lambda = 10$ nm, one would decrease α from 1.7 to 0.6. Such a variation of α may allow one to cross the transition lines of Fig. 4. Hence, we expect that the transitions described in the previous sections could be observed by means of a continuous variation of the oxygen coverage.

Finally, we notice that the small-slope approximation should be easier to reach for graphene with 12.5% oxygen (where one would require $\epsilon < \kappa_{eq}^{-1} \approx 6$ nm).

B. Carbon nanotubes

Single-carbon-nanotube electronic devices are formed via deposition of nanotubes on linear electrodes which form ripples (or grids) [14]. Assuming that the nanotube is perpendicular to the ripples, torsion energy can be neglected and our 1D model should apply. In this case, ℓ_{eq} is limited by the radius $r \sim 0.6$ nm of the nanotube [14]. Assuming once again that σ is negligible, $C = 20$ eV nm [20], and $\gamma \approx 1$ eV nm^{-1} [21], and choosing $\epsilon = 5$ nm, $\lambda = 50$ nm, one obtains $\alpha \approx 2$, which is again in the relevant range. Nevertheless, since $\epsilon \kappa_{eq} \sim 1$, slopes are not small and we do not expect quantitative accuracy of the model.

As an additional remark, the persistence length of nanotubes is $L_p = C/k_B T \approx 800$ nm, which is much larger than the

wavelength $\lambda = 50$ nm considered here. Therefore, thermal fluctuations of a free nanotube (i.e., far from the surface) are negligible at the scale of the patterns. Furthermore, the adhesion energy γ of the nanotube increases the energy cost of the fluctuations, and should lead to even smaller fluctuations for those filaments who partially or totally adhere to the surface. Therefore, fluctuations are essentially negligible at room temperature.

Finally, we have focused on single-wall carbon nanotubes because of their technological relevance, but a number of other filaments could exhibit similar behavior, such as multiwall carbon nanotubes, actin filaments, microtubules, etc.

C. Lipid membranes

The main motivation for the study of lipidic membranes is to mimic cell membrane properties within a simple system. Vesicles (i.e., closed membranes) may also be used to encapsulate molecules for targeted drug delivery or for microfluidics. In all cases the interaction of membranes with the surfaces plays an important role.

In the case of lipid membranes [8], $C = 1.4 \times 10^{-19}$ J, and $\sigma = 1.7 \times 10^{-5}$ J m^{-2} [4]. From the competition between van der Waals and hydration forces [8], $\gamma = 5 \times 10^{-6}$ J m^{-2}, and the equilibrium distance is $\ell_{eq} = 3$ nm.

Choosing $\epsilon \approx 20$ nm, and $\lambda \approx 200$ nm, we find $\alpha \approx 0.6$ and $\beta \approx 2.2$, in the range where transitions occur. Moreover, the small-slope approximation is valid ($\epsilon \kappa_{eq} \approx 0.17 < 1$, and $\sigma \gg \gamma$).

The lengthscale $d = (C/\sigma)^{1/2}$ is the cutoff length scale above which curvature energy is negligible, and the behavior is dominated by tension. Using the numerical value of the parameters given above, we find $d \approx 91$ nm. Using the results of Sec. IV B 2 when $\lambda \gg d$ (i.e., $\beta \gg 1$ or $C \ll \lambda^2 \sigma$), it is found that $(\epsilon/\lambda)_e \approx 0.12$ and $(\epsilon/\lambda)_0 \approx 0.15$. Since these aspect ratios are smaller than 1, the small-slope condition is not violated, and the transition should be observable. A typical example of pattern parameters is $\lambda = 2$ μm and $\epsilon = 0.2$ μm.

Thermal fluctuations, which have not been considered in the present study, are usually important for liquid membranes. Below the unbinding transition of the membrane [22,23], fluctuations should, to leading order, give rise to a renormalization of the model parameters (σ, C, and γ), and our model could still apply, at least qualitatively. In addition, entropic interactions between the membrane and the surface, decreasing as h^{-2}, should also play a role. An explicit analysis of thermal fluctuations should provide a more precise picture of the behavior of liquid membranes. As an example, thermal excitations could induce a mixture of the different steady states that we found at zero temperature. At low temperature, one expects a mixture of the zero-temperature ground state with the steady states having the lowest energies. Finally, the thermal behavior is expected to depend strongly on dimensionality. Hence, filaments and membranes

are expected to exhibit qualitatively different temperature behaviors.

Gravity was also neglected in the present work. The effect of the weight of the membrane or filament would in general be small for microscopic objects such as those considered in the present study. Nevertheless, gravity could be relevant in the case of a membrane separating two fluids of different densities. Indeed, this effect is already known to alter the equilibrium shape of giant vesicles [24]. The total gravitational energy in the presence of a gravity acceleration g directed along $-\hat{z}$ [with $(\hat{x}, \hat{y}, \hat{z})$ forming an orthonormal reference frame] is

$$\mathcal{E}_g(h) = g \int dx \int dy \int dz\, z\rho(x,y,z), \tag{38}$$

where we have defined the density ρ such that $\rho(x,y,z) = \rho_+$ when $z > h(x,y)$ and $\rho(x,y,z) = \rho_-$ when $z < h(x,y)$. We then have

$$\mathcal{E}_g(h) - \mathcal{E}_g(h=0) = \frac{g\Delta\rho}{2} \int dx \int dy\, h(x,y)^2, \tag{39}$$

where $\Delta\rho = \rho_- - \rho_+$. A simple dimensional analysis shows that gravity will dominate tension at length scales larger than

$$\mathcal{L}_{\sigma g} = \left(\frac{\sigma}{\Delta\rho g} \right)^{1/2}, \tag{40}$$

and gravity will dominate bending rigidity at length scales larger than

$$\mathcal{L}_{Cg} = \left(\frac{C}{\Delta\rho g} \right)^{1/4}. \tag{41}$$

Gravity will therefore be relevant at length scales larger than $\max(\mathcal{L}_{\sigma g}, \mathcal{L}_{Cg})$. Usually, $\Delta\rho$ is smaller than the density of water, i.e., $\Delta\rho < 10^3$ kg m^{-3}. Using this inequality and the above-mentioned values for σ and C, we obtain $L_{\sigma g} > 30$ μm and $\mathcal{L}_{Cg} > 2$ μm. We may therefore conclude that gravity is irrelevant for the patterns that we have considered above, for which $\lambda \lesssim 2$ μm.

VI. CONCLUSION

We have discussed the adhesion of membranes and filaments on a rippled surface within a simple 1D model. The most striking features obtained here are (1) infinite staircases of periodic ground states; (2) decimation sequences for metastable states on the fakir-carpet surface; (3) ground states that can either be the only possible steady state or coexist with a large number of metastable states. This is expected to have important consequences for binding and unbinding dynamics.

Due to the nonlinear character of the model, we have no simple tool to analyze the general case, where the pattern profile is arbitrary. Nevertheless, by working out a number of specific examples, we hope to understand which features are generic and which are not. As an example, sawtooth patterns and patterns with square crenellations exhibit a larger number of solutions than the patterns studied in the present paper

---

[4]Following the usual notations in the literature on lipid membranes, we shall here use joules and meters instead of eV and angstroms.

[25]. Nevertheless, results (1)–(3) are also obtained for saw-tooth, and square patterns [25], suggesting that these features should occur for a wide range of pattern shapes.

Also, we have seen in Sec. V that the small-slope approximation is not always verified in various systems. Hence, the analysis of the fully nonlinear problem beyond the small slope approximation, along the lines of Refs. [26,27], is an important line of future investigation.

Our results show that, in addition to chemical treatment or attachment of ligand-receptor pairs [28], geometrical patterning appears as an alternative route toward the control of adhesion of soft matter. We hope that these results will give some hints toward the understanding of adhesion of more complex systems, where the assumptions of the present model do not directly apply, such as biological membranes [29], graphene on rough surfaces [3,4], or filaments and biofilaments [30] with torsion.

APPENDIX A: VARIATION OF THE TOTAL ENERGY

For the sake of simplicity, the membrane is assumed to have only one contact point at the arclength coordinate $s = s_B$. The shape of the membrane is free for $s < s_B$, and follows the fixed shape of the surface for $s > s_B$. The total energy reads

$$\mathcal{E} = \int^{s_B} ds \left(\frac{C}{2} \kappa^2 + \sigma \right) + \int_{s_B} ds \left(\frac{C}{2} \kappa^2 + \sigma - \gamma \right). \quad \text{(A1)}$$

An additional constraint is needed to make the model complete: the membrane cannot form an angle at the contact point. Otherwise, the curvature energy would diverge. Therefore

$$\mathbf{t}_{s_B^-} = \mathbf{t}_{s_B^+}, \quad \text{(A2)}$$

where $\mathbf{t} = \partial_s \mathbf{r}$ is the unit tangent vector along the membrane. Since several quantities are discontinuous through the point at $s = s_B$, we indicate whether it is taken on the − free side, or + adhering side, with the notation $s_B^{\pm}$.

Let us now assume a variation $\delta \mathbf{r}(s)$ of the position of the curve. Tangential displacements of the curve along itself do not change the energy, and we shall assume that $\delta \mathbf{r} \cdot \mathbf{t} = 0$. Moreover, since the shape of the surface is fixed, $\delta \mathbf{r}(s) = 0$ for $s > s_B$. The variation of the energy then reads

$$\delta \mathcal{E} = \int^{s_B} ds (\delta \mathbf{r} \cdot \mathbf{n}) \left(C \partial_{ss} \kappa + \frac{C}{2} \kappa^3 - \sigma \kappa \right)$$

$$+ \left[-(\delta \mathbf{r} \cdot \mathbf{n}) C \partial_s \kappa + (\partial_s \delta \mathbf{r} \cdot \mathbf{n}) C \kappa \right]|_{s_B^-} + ds_B$$

$$\times \left[\left(\frac{C}{2} \kappa^2 + \sigma \right) \bigg|_{s_B^-} - \left(\frac{C}{2} \kappa^2 + \sigma - \gamma \right) \bigg|_{s_B^+} \right],$$

$$\text{(A3)}$$

where ds_B is the change of arclength coordinate of the contact point. The normal vector $\mathbf{n}$ points downward (i.e., toward the solid) in Fig. 1(a). With this sign convention, we have $\partial_s \mathbf{t} = \kappa \mathbf{n}$ and $\partial_s \mathbf{n} = -\kappa \mathbf{t}$.

At equilibrium, $\delta \mathcal{E} = 0$ for any $\delta \mathbf{r}$. Hence, the quantity proportional to $\delta \mathbf{r} \cdot \mathbf{n}$ in the integral must vanish, leading to Eq. (2). Moreover, the boundary terms in Eq. (A3) must also vanish. We shall see in the following section how they determine the boundary conditions.

APPENDIX B: BOUNDARY CONDITIONS

1. BC1: Smooth surface

Since no perturbation of the surface is allowed, $\delta \mathbf{r} \cdot \mathbf{n} \to 0$ at $s \to s_B$. Therefore, the term proportional to $\delta \mathbf{r} \cdot \mathbf{n}$ in the boundary terms of Eq. (A3) vanishes.

In order to combine the remaining terms, we shall first rewrite $\partial_s \delta \mathbf{r} \cdot \mathbf{n}$ in a form similar to that of the other terms. The position of the membrane before and after the perturbation is respectively denoted as $\mathbf{r}^1(s)$ and $\mathbf{r}^2(s)$, so that $\delta \mathbf{r}(s) = \mathbf{r}^2(s) - \mathbf{r}^1(s)$.

Before perturbation, the contact point is located at $s = s_B^1$, and after the perturbation, it is located at $s = s_B^2$. We expand $\mathbf{r}$ on the free side of the membrane in the vicinity of the contact point:

$$\mathbf{r}^i(s) \approx \mathbf{r}^i(s_B^i) + (s - s_B^i)\mathbf{t}_B^i + (1/2)(s - s_B^i)^2 \mathbf{n}_B^i \kappa_B^i, \quad \text{(B1)}$$

where $i = 1, 2$, and where $\mathbf{t}_B^i$, $\mathbf{n}_B^i$, and κ_B^i are the tangent vector, normal vector, and curvature at the contact point. Taking the derivative of Eq. (B1), we obtain

$$\partial_s \delta \mathbf{r}(s) \approx \mathbf{t}_B^2 - \mathbf{t}_B^1 + (s - s_B^2)\mathbf{n}_B^2 \kappa_B^2 - (s - s_B^1)\mathbf{n}_B^1 \kappa_B^1. \quad \text{(B2)}$$

From this relation, we find

$$\partial_s \delta \mathbf{r}(s_B^1) \cdot \mathbf{n}_B^1 = \mathbf{t}_B^2 \cdot \mathbf{n}_B^1 + (s_B^1 - s_B^2)\kappa_B^2 \mathbf{n}_B^2 \cdot \mathbf{n}_B^1. \quad \text{(B3)}$$

Since the tangent of the membrane at the contact point is also that of the surface, one may expand

$$\mathbf{t}_B^2 = \mathbf{t}_B^1 + (s_{0B}^2 - s_{0B}^1)\kappa_{0B}^1 \mathbf{n}_B^1, \quad \text{(B4)}$$

where s_{0B}^i is the arclength coordinate of the contact point along the surface, and κ_{0B}^i is the curvature of the surface at the contact point. To leading order $(s_{0B}^2 - s_{0B}^1) \approx (s_B^2 - s_B^1)$, $\kappa_B^2 \approx \kappa_B^1$, and $\mathbf{n}_B^2 \cdot \mathbf{n}_B^1 \approx 1$. Hence, we finally obtain

$$\partial_s \delta \mathbf{r}(s_B^1) \cdot \mathbf{n}_B^1 \approx (s_B^2 - s_B^1)(\kappa_{0B}^1 - \kappa_B^1). \quad \text{(B5)}$$

Going back to previous notation, we have $(s_B^2 - s_B^1) = ds_B$, $\kappa_{0B}^1 = \kappa|_{s_B^+}$, and $\kappa_B^1 = \kappa|_{s_B^-}$. Using Eq. (B5), the cancellation of the boundary term of the energy variation (A3) reads

$$0 = C\kappa_{s_B^-} ds_B (\kappa|_{s_B^+} - \kappa|_{s_B^-}) + ds_B$$

$$\times \left[\left(\frac{C}{2} \kappa^2 + \sigma \right) \bigg|_{s_B^-} - \left(\frac{C}{2} \kappa^2 + \sigma - \gamma \right) \bigg|_{s_B^+} \right], \quad \text{(B6)}$$

which simplifies to

$$\kappa_{s_B^-} = \kappa_{s_B^+} - \kappa_{\text{eq}}, \quad \text{(B7)}$$

where $\kappa_{\text{eq}} = (2\gamma/C)^{1/2}$. Note that the other solution $\kappa_{s_B^-} = \kappa_{s_B^+} + \kappa_{\text{eq}}$ is eliminated because it penetrates the solid.

2. BC2: Angle with adhesion on one side

In the case where the contact point is at an angle, with the membrane adhering on one side of the angle, the boundary term of the variation takes the same form as in Eq. (B6). But the variation of the contact point can only be performed on one side, so that $ds_B \geq 0$. Stability implies that the displacement of the contact point will increase the energy, i.e. the RHS of Eq. (B6) must be positive. This leads to the following boundary condition

$$\kappa_{s_B^+} - \kappa_{\text{eq}} \leq \kappa_{s_B^-} \leq \kappa_{s_B^+} + \kappa_{\text{eq}}. \tag{B8}$$

3. BC3: Point contact at an angle

In the last case, the membrane is in contact with the solid surface at one point only. Let us assume that the reaction force exerted by the surface on the membrane is $\mathbf{f}$. The variation is derived in the same way as before, except that the shape of the membrane is free on both sides. At equilibrium, the energy variation due to an infinitesimal displacement of the contact point should vanish, so that

$$\mathbf{f} \cdot \delta\mathbf{r} = [-(\delta\mathbf{r} \cdot \mathbf{n})C\partial_s\kappa + (\partial_s\delta\mathbf{r} \cdot \mathbf{n})C\kappa]|_{s_B^+} - [-(\delta\mathbf{r} \cdot \mathbf{n})C\partial_s\kappa$$
$$+ (\partial_s\delta\mathbf{r} \cdot \mathbf{n})C\kappa]|_{s_B^-}. \tag{B9}$$

This equality is true for any $\delta\mathbf{r}$, so that

$$\mathbf{f} = -\mathbf{n}(C\partial_s\kappa|_{s_B^+} - C\partial_s\kappa|_{s_B^-}),$$

$$\kappa_{s_B^+} = \kappa_{s_B^-}. \tag{B10}$$

Finally, stability simply imposes that $\mathbf{n} \cdot \mathbf{f} \geq 0$, which leads to

$$\partial_s\kappa_{s_B^+} \leq \partial_s\kappa_{s_B^-}. \tag{B11}$$

APPENDIX C: FAKIR-CARPET SURFACE

1. Structure of the solutions

Let us consider a bridge on a fakir-carpet surface. The bridge starts and ends with tangential contact points on the substrate. We shall see that the possible number of contacts of the membrane with the top of the needles (with BC3) between two tangential contact points with the bottom of the surface (with BC1) cannot be greater than 2.

To see this, we shall notice that the solutions can be classified in three symmetry classes, depending on their coefficients. These classes are shown in Fig. 6(a).

Let us consider the most complex solutions, which contain two extrema. Figure 6(b) shows all possibilities to make a bridge with these solutions. We follow the solutions from left to right. The dots indicates different parts of the solution, where the slope and the curvature have a well-defined sign. The solid arrows indicate the pieces of free solutions from one needle tip to the other. The beginning and the end of these arrows correspond to parts of the solution with equal height. The dashed arrows indicate the possible transitions with BC3 [the parts linked by the dashed arrows have the
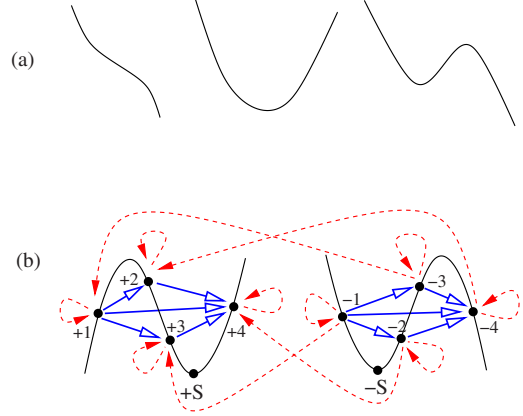

FIG. 6. (Color online) (a) Symmetry classes for the free solutions; (b) graph showing the possible bridges (see text).

same curvature; moreover, from Eq. (6), $\partial_{xxx}h$ should decrease in the direction of the arrow]. A bridge should start at one of the $\pm S$ points, run along the curve up to a black point, and then follow alternatively dashed and solid arrows, and after the last dashed arrow it must return to one of the $\pm S$ points. An inspection of this graph shows that there is no bridge with more than two contacts at the top of the needles. Considering the three types of solutions, one still obtains that the maximum number of contact points is 2.

2. Bridge solutions

We here consider the explicit solution with two contact points at the top of the two needles. The distance between the needles is denoted as $\bar{\lambda}$ (the solution with one needle is recovered for $\bar{\lambda} \to 0$). The solution involves three pieces, from left to right (i.e., along $+x$): (i) h_- from the bottom of the surface to the first needle; (ii) h_c from one needle to the other; (iii) h_+ from the second needle to the bottom of the surface.

The solution $h_-(x)$ from the bottom surface to the top of the first needle obeys $h_-(0)=0$, $\partial_x h_-(0)=0$, $\partial_{xx}h_-(0)=\kappa_{\text{eq}}$, and $h_-(x_-)=\epsilon$. Here we have chosen the origin of the x axis at the contact point with the bottom of the surface, and the needle at $x=x_-$. Using these boundary conditions in Eq. (8) leads to

$$h_-(x) = d^2\kappa_{\text{eq}}\{\cosh(x/d) - 1 + \zeta_-[\sinh(x/d) - x/d]\}, \tag{C1}$$

where ζ_- is ζ from Eq. (14), with the substitution $x \to x_-$. The slope at the needle reads

$$m_- = d\kappa_{\text{eq}}\{\sin(x_-/d) + \zeta_-[\cosh(x_-/d) - 1]\}. \tag{C2}$$

The function h_+ and the slope m_+ at the second needle are determined from a similar procedure.

The solution between the needles reads

$$h_c(x) = \epsilon + \frac{d}{2}\left((m_+ - m_-)\frac{c - \bar{c}}{\bar{s}} + (m_+ + m_-)\frac{s - (2x/\bar{\lambda})\bar{s}}{\bar{c} - (2d/\lambda)\bar{s}} \right),$$

(C3)

where $c = \cosh(x/d)$, $s = \sinh(x/d)$, $\bar{c} = \cosh(\bar{\lambda}/2d)$, and $\bar{s} = \sinh(\bar{\lambda}/2d)$, and the origin of x is now the midpoint between the needles.

Matching the curvatures at the top of the needles leads to two equations. These equations imply $f|_{x=x_+} = f|_{x=x_-}$, where

$$f = c + \zeta s + \bar{s}\frac{s + \zeta(c-1)}{\bar{c} - 2(d/\bar{\lambda})\bar{s}}.$$

(C4)

Since f is a monotonic function of x, the equation $f|_{x=x_+} = f|_{x=x_-}$ has only one solution, which is $x_+ = x_-$. Therefore $m_+ = -m_-$ and the full bridge is $x \rightarrow -x$ symmetric. Using this symmetry, and choosing $\bar{\lambda} = (n-1)\lambda$, with $x_+ = x_- = x_n$, the curvature matching condition is written as Eq. (12). The energy of the bridge is then calculated from the small-slope formula:

$$\mathcal{E}_n = \sigma[2x_n + (n-1)\lambda] + \frac{C}{2}\int dx(\partial_{xx}h)^2 + \frac{\sigma}{2}\int dx(\partial_x h)^2.$$

(C5)

In an nP state, the length of membrane in contact with the bottom of the surface between two needles is $\lambda - 2x_n$, so that the energy per period is $\mathcal{E}_n + (\sigma - \gamma)(\lambda - 2x_n)$, and the energy density reads

$$G_n = \frac{1}{n\lambda}[\mathcal{E}_n + (\sigma - \gamma)(\lambda - 2x_n)],$$

(C6)

leading to Eqs. (17) and (18).

3. Qualitative stability analysis

In this section, we would like to show that the bridge solution derived above is stable. A detailed study of stability would require a derivation of the second variation of the energy (i.e., the variation of $\mathcal{E}$ to second order in $\delta\mathbf{r}$). We shall here avoid this lengthy analysis, and proceed in a different—and more qualitative—way.

Let us assume that the bridge solution obtained above is unstable, i.e., it does not correspond to a minimum of the energy. In such a case, one could decrease the energy of the bridge by making a continuous change of its shape (including a possible change of the position of the contact points). But the total energy of a bridge solution passing over the two needles must be larger than the energy $\mathcal{E}_a$ of a membrane in adhesion along a flat substrate with no needles (indeed, the terms proportional to σ and C are minimum for a straight configuration, and adhesion the term proportional to γ is minimum for adhesion everywhere on the substrate). Therefore, the energy of the deformed bridge cannot be decreased indefinitely, and it must converge to a given value $\mathcal{E}_* > \mathcal{E}_a$. The value $\mathcal{E}_*$ then corresponds to a minimum of the energy, and the corresponding shape of the bridge must be another

bridge solution.[5] But we have seen above that there is only one bridge solution. We therefore reach a contradiction, and the bridge solution determined above corresponds to a minimum of energy.

Of course, since there are actually other needles on the surface, some solutions are forbidden because they would penetrate the surface. But this is a separate problem, which does not affect local stability.

APPENDIX D: SINUSOIDAL SURFACE

1. Bridge solutions

a. General bridge solution on smooth surfaces

We first give the form of a general solution between two contact points with BC1, at x_- and $x_+ > x_-$. Let us define

$$y = [x - (x_+ + x_-)/2]/d,$$

(D1)

$$\eta = (x_+ - x_-)/2d,$$

(D2)

$$\eta_* = (x_+ + x_-)/2d,$$

(D3)

$$\Delta(y) = h_s(y) - h_s(-y),$$

(D4)

$$\Sigma(y) = h_s(y) + h_s(-y).$$

(D5)

For given positions and slopes of the contact points, the bridge solution is unique and reads

$$\begin{aligned} h(y) = &\frac{\partial_y \Sigma(\eta)}{2\sinh\eta}(\cosh y - \cosh\eta) \\ &+ \frac{1}{2}\frac{-\Delta(\eta)/\eta + \partial_y\Delta(\eta)}{\cosh\eta - \sinh\eta/\eta}\left(\sinh y - \frac{y}{\eta}\sinh\eta\right) \\ &+ \frac{y}{2\eta}\Delta(\eta) + \frac{\Sigma(\eta)}{2}. \end{aligned}$$

(D6)

Imposing BC1 at the contact points, we obtain two conditions:

$$\frac{\partial_y\Sigma(\eta)}{\tanh\eta} = \partial_{yy}\Sigma(\eta) + 2\tilde{\kappa},$$

(D7)

$$\frac{-\Delta(\eta)/\eta + \partial_y\Delta(\eta)}{1/\tanh\eta - 1/\eta} = \partial_{yy}\Delta(\eta),$$

(D8)

where $\tilde{\kappa} = \kappa_{eq}d^2$.

b. Bridge solution for the sinusoidal surface

We now apply these formulas to the case of the sinusoidal surface, where

---

[5]This statement is not mathematically rigorous. Indeed, we have ruled out the possibility that $\mathcal{E}_*$ corresponds to a singular solution, which is outside the family of shapes that we consider for the bridges. From a close inspection of the problem, we found no candidate for such a singular solution.
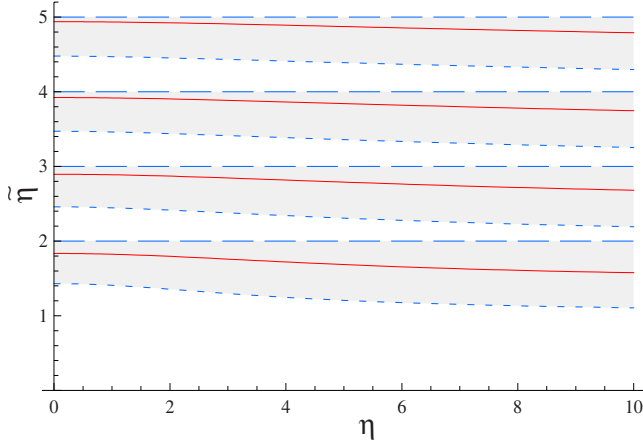
FIG. 7. (Color online) Nonsymmetric solutions are forbidden by the nonpenetration constraint. The solid lines represent the nonsymmetric sinusoidal solutions. The shaded region is the region where the solutions always penetrate the substrate. The dashed lines correspond to integer values of $\tilde{\eta}$. The dotted lines corresponds to the solutions of $\tilde{\eta} = r_m$. See text for detailed explanations.

$$h_s = -\epsilon \cos(2\pi x/\lambda). \qquad (D9)$$

Then Eq. (D7) leads to

$$\frac{A}{\cos(\pi\tilde{\eta}_*)} = -\cos(\pi\tilde{\eta}) + \frac{\beta}{2\pi \tanh \eta} \sin(\pi\tilde{\eta}), \quad (D10)$$

where

$$A = \kappa_{eq}/\kappa_g,$$

$$\tilde{\eta} = 2\eta/\beta,$$

$$\tilde{\eta}_* = 2\eta_*/\beta. \qquad (D11)$$

We have used the geometric curvature $\kappa_g = 4\pi^2\epsilon/\lambda^2$, as defined in the main text. Furthermore, the parameter A is related to α via $\alpha = |A|^{1/2}$.

The other condition (D8) leads to two types of solutions. The first ones are $x \rightarrow -x$ symmetric solutions, for which $\tilde{\eta}_* = p$, with p integer. The second are nonsymmetric solutions, obeying

$$\frac{1}{\eta}\left(\frac{1}{\tanh \eta} - \frac{1}{\eta}\right) = \frac{1}{\pi\tilde{\eta}}\left(\frac{1}{\pi\tilde{\eta}} - \frac{1}{\tan[\pi\tilde{\eta}]}\right). \qquad (D12)$$

c. Nonpenetration constraint

We shall now see how the nonpenetration constraint leads to a drastic selection of the solutions. Plotting the solutions (D6) for the sinusoidal surface, we observe that they penetrate the substrate for any value of η_* when $\tilde{\eta}$ is decreased below integer values. Decreasing again $\tilde{\eta}$, nonpenetrating solutions begin to exist for some values of η_*. The first solution to be nonpenetrating when $\tilde{\eta}$ is decreased is the symmetric solution with $\partial_{xx}h(x_+) = \partial_{xx}h_s(x_+)$. Such a condition may be written as $\tilde{\eta} = r_m$, where $m \geq 2$ is an integer and r_m is the solution of

$$\frac{1}{\eta} \tanh \eta = \pi r_m \tan(\pi r_m). \qquad (D13)$$

Finally, solutions penetrate the substrate for all values of η_* when

$$m \geq \tilde{\eta} \geq r_m \qquad (D14)$$

(note that $r_m > m-1$). Figure 7 shows that the solutions of Eq. (D12) all fall into the regions where solutions penetrate the substrate for all possible values of η_*. Therefore, the nonsymmetric solutions are forbidden.

Hence, we only have to consider symmetric solutions. We shall set $\cos(\pi\tilde{\eta}_*) = 1$, thereby considering only p even in $\tilde{\eta}_* = p$. The solutions with p odd are considered via $\epsilon \leq 0$, i.e., with $A < 0$. With these definitions, the membrane can now be on both sides of $h_s(x)$. The solutions are above the surface for $A > 0$ and below for $A < 0$. Penetrating solutions are then defined as those that cross the surface between the two contact points.

The solutions of Eq. (D10) in the $(A, \tilde{\eta})$ plane are shown in Fig. 8(a). The corresponding bridge solutions are shown in Fig. 9. The nonpenetration constraint again leads to a drastic selection of the solutions.

2. Qualitative stability analysis

Once again, we shall avoid a full derivation of the second variation of the energy, and we analyze stability of the bridge solutions within a qualitative picture. Let us assume that a change of shape can decrease the energy when the position and slope at the ends of the bridge are fixed. It is clear that the energy of the bridge must be larger than that of a straight segment between the contact points, so that $\mathcal{E} \geq \sigma(x_+ - x_-)$ for any configuration. Therefore, the energy cannot decrease indefinitely during the change of shape, and it should converge to a value $\mathcal{E}_*$, where the energy cannot be decreased further. This value is a minimum of the energy, so that the corresponding shape must be a bridge solution different from the initial one. But we have seen above that the bridge solution (D6) for fixed position and slope at the ends is unique.[6] This leads to a contradiction, and shows that a bridge solution with fixed position and slope at the ends is stable with respect to shape changes.

One therefore needs to analyze only the change of energy when the boundary points are moved along the surface. Since we know that the solutions are symmetrical, we need to vary only the length of the solution $x_+ - x_-$. Actually, we will rather vary the relative length $(x_+ - x_-)/\lambda = \tilde{\eta}$. This means that we shall analyze stability by moving vertically in the $(A, \tilde{\eta})$ plane.

We start by considering a membrane that is in adhesion everywhere along the surface, corresponding to $\tilde{\eta} = 0$. Making a bridge with an infinitesimal length $\ell = x_+ - x_-$, we increase the energy by an amount $\approx \gamma\ell$ (the changes in the tension and curvature energies are higher order in ℓ). There-

---

[6]As mentioned in Appendix C 3, such a statement lacks mathematical rigor.
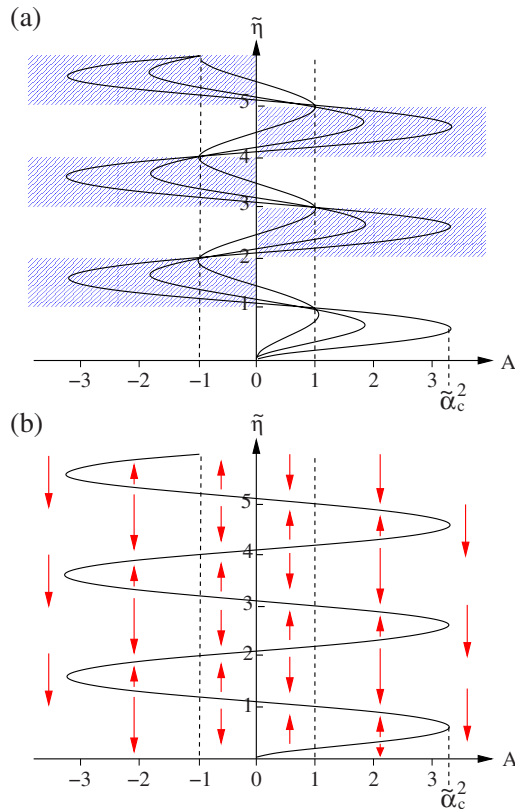
(a)

(b)

FIG. 8. (Color online) Symmetric solutions on the sinusoidal surface. (a) Solutions for $\beta = 0$, 10, and 20. The dashed regions are the regions that are forbidden due to the nonpenetration constraint. (b) Stability of the solution for $\beta = 20$. The arrows indicate the direction where energy decreases.

fore, we expect the state of complete adhesion to be a local minimum. Increasing $\tilde{\eta}$ for fixed A, the energy is then expected to increase, up to the point where a solution is reached. The first solution to be reached is therefore a maximum of energy: it is unstable. Then the energy decreases, up to a local minimum, and it increases again, up to a local maximum, etc. The results of this analysis are shown in Fig. 8(b).

3. Summary

The solutions and their stability are plotted in Fig. 8. They are classified in three regimes as a function of $\alpha = |A|^{1/2}$. (i)
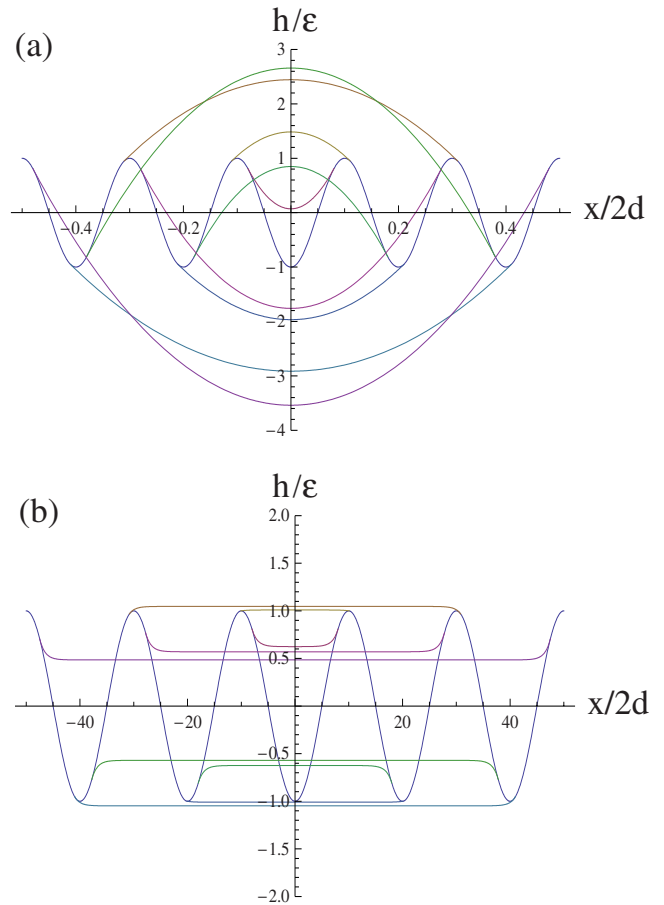

(a)

(b)

FIG. 9. (Color online) Symmetric bridge solutions. The solutions are plotted for two different values of β. (a) $\beta = 0.2$. The solution is plotted for $\tilde{\eta} = 0.8, 1.1, 1.8, 2.1, 2.8, 3.1, 3.8, 4.1, 4.8$. (b) For large values of β, bridges become flat. For $\beta = 20$, with $\tilde{\eta} = 0.8, 1.01, 1.8, 2.01, 2.78, 3.08, 3.78, 4.1, 4.75$.

For $\alpha > \tilde{\alpha}_c$, there is no solution. (ii) When $1 < \alpha < \tilde{\alpha}_c$ there is one stable, and one unstable bridge solution. Both solutions have a length smaller than λ. (iii) When $0 < \alpha < 1$, there is one unstable solution with length smaller than λ, and an infinite family of stable solutions with wavelengths larger than λ. In the main text, we account only for the stable solutions.

[1] D. Quéré, Rep. Prog. Phys. **68**, 2495 (2005).
[2] S. V. Morozov, K. S. Novoselov, M. I. Katsnelson, F. Schedin, L. A. Ponomarenko, D. Jiang, and A. K. Geim, Phys. Rev. Lett. **97**, 016801 (2006).
[3] M. Ishigami, J. H. Chen, W. G. Cullen, M. S. Fuhrer, and E. D. Williams, Nano Lett. **7**, 6 (2007).
[4] E. Stolyarova, K. T. Rim, S. Ryu, J. Maultzsch, P. K. N. L. E. Brus, T. F. Heinz, M. S. Hybertsen, and G. W. Flynn, Proc. Natl. Acad. Sci. U.S.A. **104**, 9209 (2007).
[5] M. Y. Han, B. Ozyilmaz, Y. Zhang, and P. Kim, Phys. Rev.

Lett. **98**, 206805 (2007).
[6] A. Incze, A. Pasturel, and P. Peyla, Phys. Rev. B **70**, 212103 (2004).
[7] P. S. Swain and D. Andelman, Phys. Rev. E **63**, 051911 (2001).
[8] G. Palasantzas and G. Backx, Phys. Rev. B **54**, 8213 (1996).
[9] U. Seifert and R. Lipowsky, Phys. Rev. A **42**, 4768 (1990).
[10] R. Capovilla and J. Guven, Phys. Rev. E **66**, 041604 (2002).
[11] M. Deserno and T. Bickel, Europhys. Lett. **62**, 767 (2003).
[12] C. Tordeux and J.-B. Fournier, Europhys. Lett. **60**, 875 (2002).

[13] M. Deserno, Phys. Rev. E **69**, 031903 (2004).

[14] V. Derycke, R. Martel, J. Appenzeller, and P. Avouris, Nano Lett. **1**, 453 (2001).

[15] J. Im, J. Kang, M. Lee, B. Kim, and S. Hong, J. Phys. Chem. B **110**, L12839 (2006).

[16] L. Landau and E. Lifshitz, *Theory of Elasticity* (Elsevier, Amsterdam, 1986), Vol. 7.

[17] R. Gallotti and O. Pierre-Louis, Phys. Rev. E **75**, 031801 (2007).

[18] J. W. Gibbs, *Scientific Papers 1906* (Dover, New York, 1961).

[19] E. D. Williams (private communication).

[20] M. Sano, A. Kamino, J. Okamura, and S. Shinkai, Science **293**, 1299 (2001).

[21] T. Hertel, R. E. Walkup, and P. Avouris, Phys. Rev. B **58**, 13870 (1998).

[22] R. Lipowsky and S. Leibler, Phys. Rev. Lett. **56**, 2541 (1986).

[23] R. Lipowsky, Phys. Rev. Lett. **62**, 704 (1989).

[24] M. Kraus, U. Seifert, and R. Lipowsky, Europhys. Lett. **32**, 431 (1995).

[25] O. Pierre-Louis (unpublished).

[26] M. M. Müller, M. Deserno, and J. Guven, Phys. Rev. E **76**, 011921 (2007).

[27] S. Das and Q. Du, Phys. Rev. E **77**, 011907 (2008).

[28] F. Pincet, E. Perez, J.-C. Loudet, and L. Lebeau, Phys. Rev. Lett. **87**, 178101 (2001).

[29] J. L. Tan, J. Tien, D. M. Pirone, D. S. Gray, K. Bhadriraju, and C. S. Chen, Proc. Natl. Acad. Sci. U.S.A. **100**, 1484 (2003).

[30] L. Huang, P. Manandhar, K.-E. Byun, P. B. Chase, and S. Hong, Langmuir **21**, L22 (2006).

[31] J. S. Langer, Rev. Mod. Phys. **52**, 1 (1980).